All-Semiconductor Negative-Index Plasmonic Absorbers

S. Law,[1] C. Roberts,[2] T. Kilpatrick,[1] L. Yu,[1] T. Ribaudo,[3] E. A. Shaner,[3] V. Podolskiy,[2] and D. Wasserman[1]
[1]*University of Illinois Urbana Champaign, Department of Electrical and Computer Engineering, Micro and Nanotechnology Lab, Urbana, Illinois 61801, USA*
[2]*Department of Physics and Applied Physics, University of Massachusetts Lowell, Lowell, Massachusetts 01854, USA*
[3]*Sandia National Labs, P.O. Box 5800, Albuquerque, New Mexico 87185, USA*
(Received 12 June 2013; published 6 January 2014)

We demonstrate epitaxially grown all-semiconductor thin-film midinfrared plasmonic absorbers and show that absorption in these structures is linked to the excitation of highly confined negative-index surface plasmon polaritons. Strong (>98%) absorption is experimentally observed, and the spectral position and intensity of the absorption resonances are studied by reflection and transmission spectroscopy. Numerical models as well as an analytical description of the excited guided modes in our structures are presented, showing agreement with experiment. The structures investigated demonstrate a wavelength-flexible, all-semiconductor, plasmonic architecture with potential for both sensing applications and enhanced interaction of midinfrared radiation with integrated semiconductor optoelectronic elements.

DOI: 10.1103/PhysRevLett.112.017401 PACS numbers: 78.67.Pt, 42.25.Bs, 78.30.Fs, 78.66.Fd

There has been significant recent interest in so-called "perfect" absorber (PA) structures, metamaterial structures that demonstrate spectrally selective near-unity absorption at predefined resonant wavelengths. Initial PA structures were demonstrated in the microwave range using a resonator or wire structure [1]. The concept was subsequently expanded to optical frequencies with plasmonic resonator structures [2] and, more recently, subwavelength plasmonic discs [3] and stripes [4] separated from an optically thick metallic ground plane by a thin dielectric spacer. The absorption mechanism for such structures has been described in terms of impedance matching [1], critical coupling [4], and more recently by interference [5]. In this Letter, we present all-semiconductor highly compact PAs that operate by coupling incident diffraction-limited mid-IR light into exotic negative-index surface modes supported by submicron waveguides, predicted in Refs. [6–8] and demonstrated at visible wavelengths in Ref. [9].

Perfect absorbers are structures whose efficiency comes from engineering the very losses that serve as obstacles for so many other applications of plasmonics and metamaterials. The potential for PA applications is especially evident in the midinfrared (mid-IR) wavelength range (2–30 μm), where all finite temperature biological and mechanical objects emit thermal radiation, where numerous molecules have fundamental absorption resonances, and where the ability to engineer the optical properties of materials has the potential to significantly impact sensing, defense, and security applications. Surfaces with strong absorption resonances could find use as selective thermal emitters for thermophotovoltaic or thermal cloaking or mimicry applications. Alternatively, PA structures could potentially be utilized to enhance the interaction of incident light with molecules of interest or with subwavelength pixels for focal plane array thermal imaging. The structures presented here, being all semiconductor in nature, are especially intriguing for integration with mid-IR opto-electronic devices.

Perfect absorption (or the equivalent selective thermal emission) has been demonstrated at these longer wavelengths using metamaterial resonators [10,11] and either metallic stripes [12] or discs [13] acting as optical antennas. The above examples all use the same plasmonic metals (Ag, Au) used in shorter wavelength PA structures. However, at longer wavelengths, these traditional plasmonic metals' optical properties resemble those of perfect electrical conductors (large, negative real part of ϵ), limiting the utilization of phenomena associated with composite materials having metal and dielectric permittivities of the same order of magnitude ($|\epsilon_m| \approx |\epsilon_d|$). Recently, it was demonstrated that highly doped semiconductors can be engineered to behave, in the mid-IR region, similarly to traditional plasmonic metals such as Au and Ag at shorter wavelengths [14–16], allowing for the fabrication of subwavelength structures supporting mid-IR localized surface plasmons [17,18] as well as for potential integration into all-semiconductor active mid-IR plasmonic devices [19]. In addition, the permittivity of these "engineered" plasmonic materials can quite accurately be modeled by the Drude formalism for a broad range of frequencies (including $\omega \geq \omega_p$ where $\epsilon_m \approx 0$ and $\epsilon_m > 0$), which is not possible with traditional plasmonic metals due the effects of interband transitions (and thus absorption resonances) at frequencies near and greater than the plasma frequency (ω_p). In this sense, these engineered plasmonic materials are "purer" than their short-wavelength counterparts, and some phenomena difficult to observe near the plasma frequency for Au and Ag (at shorter wavelengths) can result in striking optical properties near ω_p for composite material

systems employing heavily doped semiconductors (at longer wavelengths).

Here, we demonstrate an all-semiconductor plasmonic (near-perfect) absorber using highly doped ($n = 6.9\times 10^{19}$ cm^{-3}) InAs as the plasmonic material. Strong absorption is achieved by coupling into negative-index, highly confined surface plasmon polariton modes in a multilayer epitaxial structure. We show that whereas the resonant behavior of these structures depends weakly on their lateral geometry, control over the spatial profile of the optical mode and the intensity of the absorption resonance can be achieved by varying the vertical profile and excitation wavelength of structures fabricated from the same epitaxial growth. Furthermore, our absorption is achieved in an architecture designed to allow, depending again on the vertical profile of the absorber and the excitation wavelength, either integration with active semiconductor elements or enhanced interaction with molecular species on the PA surface, enabling the development of mid-IR all-semiconductor-based plasmonic devices for sensing and optoelectronic applications.

Our material system, shown in Fig. 1 (inset), was grown by molecular beam epitaxy and optically characterized by infrared reflection and transmission spectroscopy. The as-grown structure was modeled with both analytical (T-matrix) and numerical finite difference time domain (FDTD) techniques [20,21], and the doped layers' optical properties modeled using the Drude formalism, with only the scattering rate and plasma frequency as the fitting parameters. Figure 1 shows the experimental transmission and reflection from our as-grown material as well as the numerically and analytically calculated spectra for the same structure. Our T-matrix and FDTD calculations faithfully reproduce the experimental reflection results, indicating that our doped InAs can accurately be described using the Drude formalism, from which we can extract the frequency-dependent permittivity of our $n+$ doped InAs layer. Our modeled transmission matches the experimental transmission spectral shape but does not accurately replicate the observed transmission magnitude, an effect seen in previous work and attributed to losses due to the high defect density at the lattice-mismatched InAs/GaAs interface [17,22].

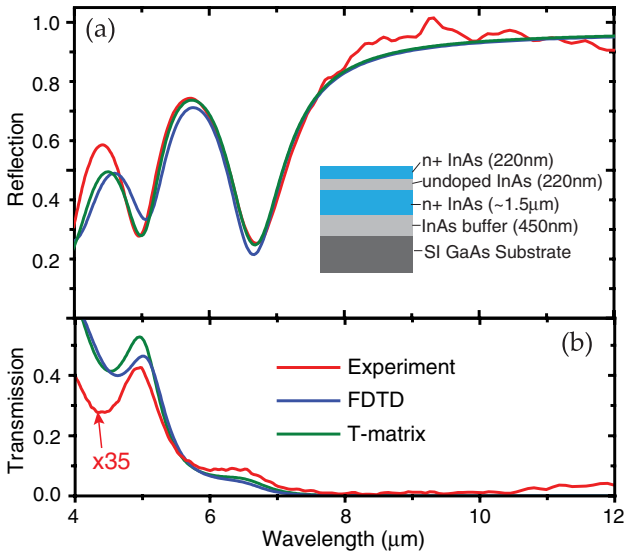

FIG. 1 (color online). Experimental (red lines), numerically modeled (blue lines), and T-matrix calculated (green lines) (a) reflection and (b) transmission spectra for the unpatterned, as-grown perfect absorber sample. Experimental transmission has been scaled by ×35. Inset shows a schematic of the sample epitaxial layer structure.

Perfect absorbers were fabricated by etching stripes into our as-grown material. The resulting structures' optical responses are polarization dependent, such that only TM polarized incident light [as shown in Fig. 2(b)] will demonstrate strong absorption resonances. Whereas a two-dimensional (2D) surface pattern could potentially give polarization insensitive absorption, the underlying physics of both the one-dimensional (1D) and 2D patterns is essentially identical, with the 1D array giving the added benefit of allowing us to compare the TE and TM reflection from our sample, isolating the PA resonance from any other optical effects observed from our multilayer structure. See the Supplemental Material for details of growth, fabrication, and experimental optical characterization [23].

Figure 2(a) shows the reflection spectra for TM and TE polarized light, respectively, from a PA sample with periodicity $\Lambda = 4$ μm, stripe width $w = 2.1$ μm, and etch depth $d = 210$ nm, shown in the schematic and atomic force micrograph in Figs. 2(b) and 2(c). As can be seen in the TM-polarized spectra, a sharp dip in reflection is observed at ~7.75 μm. No corresponding feature is observed in the TE-polarized reflection spectra or in the transmission spectra, indicating that the observed feature is, in fact, an

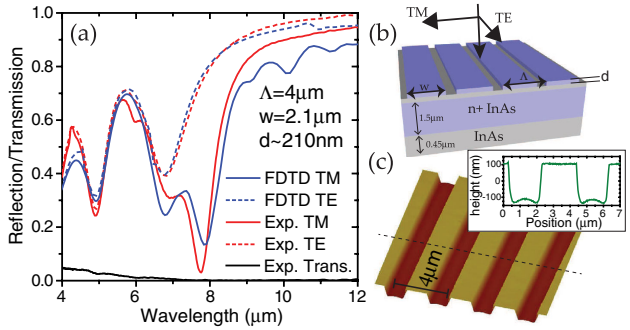

FIG. 2 (color online). (a) TM (solid lines) and TE (dotted lines) experimental (red) and FDTD calculated (blue) reflection for a PA sample with $\Lambda = 4$ μm, $w = 2.1$ μm, and $d = 210$ nm. Experimental transmission is shown in black. (b) Schematic of PA absorber structure and (c) atomic force micrograph (AFM) of the PA characterized in (a), with inset showing an AFM line scan (dashed line) across the sample surface.

absorption peak resulting from our semiconductor plasmonic structure. The PA was also modeled using FDTD [shown in blue in Fig. 2(a)], and agreement with our experimental results is demonstrated.

Both TE and TM reflection spectra were obtained for samples with varying fill factors and periodicities. Figure 3(a) shows a scatter plot of the characterized samples' absorption (calculated as $1 - R_{TM}/R_{TE}$ at resonance) as a function of fill factor (x axis) and etch depth (color scale), as determined by AFM. The spectral position of the observed absorption peaks remained relatively constant (within ± 250 nm of $\lambda = 7.72$ μm) for a wide range of lateral geometries with approximately constant etch depths, as seen in the TM spectra shown in Fig. 3(b). However, whereas lateral geometry only weakly affects the spectral position of our resonant absorption, a wide variation in absorption intensities was observed (from 0% to 98.7%) absorption) across the fabricated samples [Fig. 3(a)], seemingly independent of lateral geometry.

Figure 3(c) shows the experimental absorption intensity (red squares) for all of the fabricated samples as a function solely of etch depth. This scatter plot is compared to FDTD simulations (blue stars) of a representative sample with $\Lambda = 4$ μm, $w = 2.4$ μm, and varying etch depths. The experimental absorption correlates strongly with the etch depth of the sample, a trend also observed in the simulation results. Because a wet etch was used, a wide variation in etch depths was observed among the samples. All but one sample etched within 20 nm of the top layer thickness ($200 < d < 240$ nm) demonstrated absorption of $> 90\%$. However, as the etch depth penetrates into the undoped material, a significant decrease in absorption is seen, with no absorption peak observed, and total absorption of $\sim 30\%$, for samples with etch depths $350 < d < 500$ nm. For these samples, TM reflection spectra closely approximate their TE counterparts. For $d > 550$ nm, the absorption peak reappears, with the most deeply etched sample ($d = 1.1$ μm) again showing absorption $> 90\%$. Figure 3(d) shows the TE and TM reflection spectra for representative samples with similar fill factors (w/Λ) and varying etch depths.

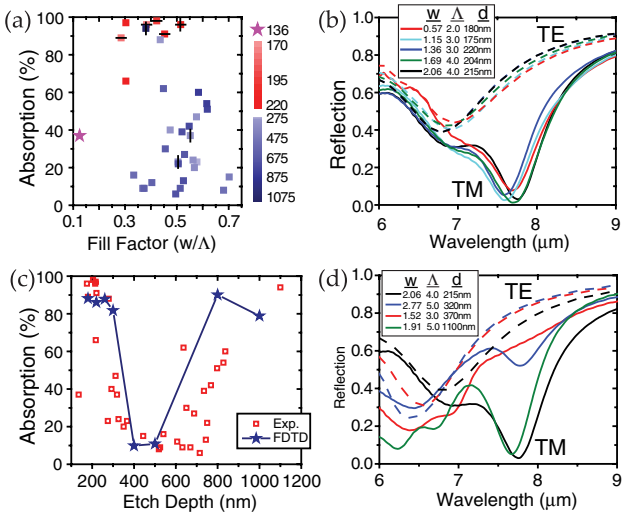

FIG. 3 (color online). (a) Scatter plot showing experimental absorption intensity ($1 - R_{TM}/R_{TE}$) at resonance for a range of samples as a function of fill factor (x axis) and etch depth in nm (color scale). (b) TE (dashed lines) and TM (solid lines) experimental reflection spectra for features [marked with horizontal lines in (a)] with a range of lateral geometries and etch depths between 180 and 220 nm. (c) Experimental (red squares) and modeled (blue stars) absorption for all features characterized as a function solely of etch depth. Modeled data use samples with $\Lambda = 4$ μm and $w = 2.4$ μm and varying etch depth d. (d) TE (dashed lines) and TM (solid lines) experimental reflection spectra for samples with similar fill factor and varying etch depth d [marked with vertical lines in (a)].

Note that unlike the conventional antenna resonances observed in Refs. [11] and [12], the observed resonances do not scale linearly with individual stripe size. Detailed analysis of the electromagnetic response of our PA structures reveals a different absorption mechanism than that in previously reported perfect absorber structures. To provide quantitative analysis of light interaction with patterned all-semiconductor systems, Maxwell's equations were numerically solved with FDTD [20] and rigorous coupled wave analysis [24] techniques. The results of these calculations largely agree with the observed experimental data. The field distribution pattern and analysis of the dependence of absorption on geometric parameters of the system (w, Λ, d) suggests that the PA behavior is related to the resonant light coupling into modes guided by the layered structure.

Dispersion of the guided modes supported by the layered semiconductor materials was calculated using the T-matrix technique (Fig. 4) [25] for three different configurations: metal-dielectric-metal (MDM), corresponding to the as-grown epitaxial structure, air-dielectric-metal (ADM), corresponding to the as-grown material structure with the top doped InAs layer removed, and air-metal-dielectric-metal (AMDM), corresponding to the case where the top layer is partially ($d = 110$ nm) removed (here "metal" refers to the $n+$ InAs layers). In this approach, Maxwell's equations are solved for the reflectivity of the multilayer stack for fixed frequency as a function of the component of the incident wave vector parallel to the layers. Guided modes correspond to the condition of infinite stack reflectivity. Here, we calculate the (complex) frequency spectra of the modes as a function of the in-plane wave vector component. Dispersion of the guided modes in the layered system is shown in Fig. 4(a). These calculations revealed a family of highly confined and also highly lossy (with lifetimes of the order of 170 fs, or ~ 6 periods of oscillations) plasmon waves supported by the layered system in the frequency range between ~ 7 and ~ 8.3 μm, corresponding to the condition $-\epsilon_{InAs} \leq \mathrm{Re}(\epsilon_m) \leq -1$ (with ϵ_{InAs} being the undoped InAs permittivity and $\mathrm{Re}(\epsilon_m)$ being the real part of

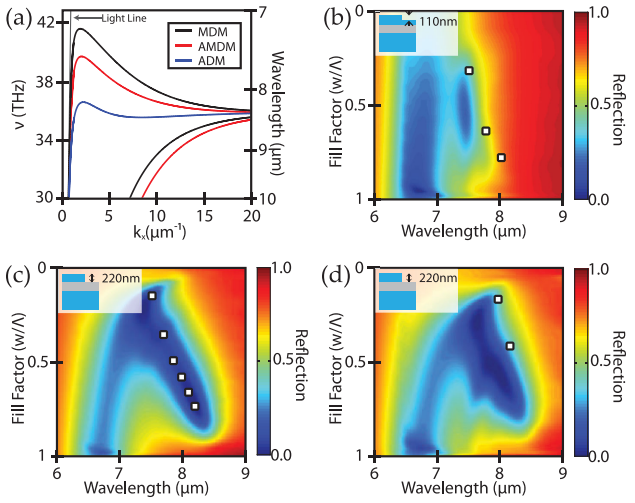

FIG. 4 (color online). (a) Dispersion relations of the guided modes supported by the noncorrugated stacks. Black, blue, and red curves correspond to MDM, ADM, and undercut AMDM structures; thin gray line represents dispersion of the plane wave in vacuum. Note that the high-index modes have negative refractive index for shorter wavelength and positive index for longer wavelength. (b)– (d) Reflection spectrum for different etch depths and periodicity as a function of fill factor and wavelength. The parameters for the plots are (b) $\Lambda = 2\ \mu$m, $d = 110$ nm, (c) $\Lambda = 4\ \mu$m, $d = 220$ nm, (d) $\Lambda = 2\ \mu$m, $d = 220$ nm; white squares correspond to spectral positions of intersections of collective resonances formed by guided modes in corrugated systems and fundamental half-wavelength resonances of AMDM (b) and ADM [(c) and (d)] modes.

the doped InAs permittivity). In contrast to the majority of optical guided modes, the waves supported by the doped semiconducting structures have a very large refractive index, which translates into their slow group velocity. A peculiar property of these waves is that they have negative index, in the sense that the in-plane component of the wave vector points opposite to the in-plane component of the Poynting flux [8]. However, in contrast to previous studies [9] that focused on refraction of these modes, here we utilize diffraction of incoming plane waves into these waves to engineer strong absorption.

Our analysis shows that the position of absorption resonances can be related to the properties of these guided modes. In fact, for normal incidence, the position of the major absorption resonances can be traced to the spectral overlap of (i) the fundamental (1/2 local wavelength) resonance of the relatively "low-index" ADM/AMDM mode and (ii) the odd-half-wavelength resonance of its "high-index" MDM counterpart. Such a combination essentially results in resonant excitation of a plasmonic-crystal-type collective mode in the periodic ADM (AMDM)-MDM structure [26] [spectral positions of such resonances are shown in Figs. 4(b)–4(d)]. Evolution of these plasmonic-crystal modes defines the observed PA response.

The variation of etch depth effectively modifies the spectrum of available waves (primarily by modulating the dispersion of ADM/AMDM modes) and also controls coupling to these plasmonic modes. For small values of d, the guided mode of the structure comprises a combination of the AMDM and MDM modes. As the etch depth increases past $d \simeq 220$ nm, the guided mode transforms into a superposition of the ADM/MDM modes, resulting in the strong absorption observed in our experiments. Such structures efficiently couple incident light into the subwavelength undoped InAs waveguides and have potential applications for enhancing the interaction of long wavelength light with thin optoelectronic active regions in detectors or emitters. Coupling to very high index guided modes is often higher-order coupling ($k_x^{\mathrm{mode}} - \omega/c = m2\pi/\Lambda$ with $m > 1$). In our samples, light preferentially couples to the $m \simeq 2$ diffraction orders, corresponding to $\lambda_0 \sim 7.5\ \mu$m; $w/\Lambda \simeq 0.4$ in Figs. 4(c) and 4(d). As the etch depth increases to $d \simeq 440$ nm, the ADM mode disappears, which effectively destroys the collective guided mode. Further increase of the etching allows the MDM mode to couple with "positive-index" surface plasmon polaritons supported by the air-doped InAs interface; however, since the field confinement in this wave is much weaker than in its ADM counterpart, substantial overlap between the fields of the MDM and surface plasmon polariton modes (required for the creation of the collective plasmonic crystal mode) can be only achieved at deeper etch depth. See the Supplemental Material for details on the calculations of guided mode lifetimes, dependence on etch depth, resonant absorption wavelength, and coupling conditions [23].

The available spectrum of guided waves also defines the angular sensitivity of the observed absorption phenomenon. Our analysis demonstrates that the absorption strength of samples with smaller period is relatively insensitive to the incident angle of the excitation. At the same time, the spectral positions of the absorption maxima in samples with larger period ($\Lambda \sim 5\ \mu$m) exhibit substantial modulation with incident angle related to (i) coupling to negative-index modes with different m values and (ii) coupling to low-positive-index modes at higher wavelength. Ultimately, the angular dependence of our samples results from the momentum matching conditions for coupling into the guided modes of the system. Larger periodicities of the patterned top layer, coupling into available lower order modes, gives smaller grating momenta ($G = m2\pi/\lambda$) and, thus, a larger relative effect from changing the incidence angle of the excited light. See the Supplemental Material, where reflection spectra for two samples ($\Lambda = 2\ \mu$m and $\Lambda = 5\ \mu$m) are simulated for a range of incidence angles [23].

In summary, we have demonstrated all-semiconductor plasmonic absorber structures with absorption resonances showing greater than $> 98\%$ absorption and explained the observed behavior as resulting from the resonant excitation of negative-index surface modes. The spectral

position of our absorption resonance is shown to be effectively independent of device geometry, and the absorption strength is shown to be highly dependent on the etch depth of the top patterned layer. The strong absorption of light in the structures' subwavelength volumes holds promise for integration with semiconductor optoelectronic devices lattice matched to InAs or GaSb, such as detectors or lasers, or alternatively, for fundamental investigations of light-matter interactions between electronic resonances in semiconductor heterostructures and the observed plasmonic resonances.

This work was supported by the AFOSR Young Investigator Program (Grant No. FA9550-10-1-0226) and the NSF MWN program (Grants No. DMR-1209761 and No. DMR-1210398). Sandia is a multiprogram laboratory operated by Sandia Corporation, a Lockheed Martin Company, for the United States Department of Energy's National Nuclear Security Administration under Contract No. DE-AC04-94AL85000.

[1] N. I. Landy, S. Sajuyigbe, J. J. Mock, D. R. Smith, and W. J. Padilla, Phys. Rev. Lett. **100**, 207402 (2008).
[2] Y. Avitzour, Y. A. Urzhumov, and G. Shvets, Phys. Rev. B **79**, 045131 (2009).
[3] N. Liu, M. Mesch, T. Weiss, M. Hentschel, and H. Giessen, Nano Lett. **10**, 2342 (2010).
[4] C. Wu, B. Neuner, G. Shvets, J. John, A. Milder, B. Zollars, and S. Savoy, Phys. Rev. B **84**, 075102 (2011).
[5] H. T. Chen, J. Zhou, J. F. O'Hara, F. Chen, A. K. Azad, and A. J. Taylor, Phys. Rev. Lett. **105**, 073901 (2010).
[6] E. N. Economou, Phys. Rev. **182**, 539 (1969).
[7] P. Tournois and V. Laude, Opt. Commun. **137**, 41 (1997).
[8] V. Agranovich, Y. Shen, R. Baughman, and A. Zakhidov, J. Lumin. **110**, 167 (2004).
[9] H. J. Lezec, J. A. Dionne, and H. A. Atwater, Science **316**, 430 (2007).
[10] Z. H. Jiang, S. Yun, F. Toor, D. H. Werner, and T. Mayer, ACS Nano **5**, 4641 (2011).
[11] X. Liu, T. Tyler, T. Starr, A. F. Starr, N. M. Jokerst, and W. J. Padilla, Phys. Rev. Lett. **107**, 045901 (2011).
[12] J. A. Mason, S. Smith, and D. Wasserman, Appl. Phys. Lett. **98**, 241105 (2011).
[13] J. A. Mason, G. Allen, V. A. Podolskiy, and D. Wasserman, IEEE Photonics Technol. Lett. **24**, 31 (2012).
[14] J. C. Ginn, R. L. Jarecki, E. A. Shaner, and P. S. Davids, J. Appl. Phys. **110**, 043110 (2011).
[15] M. Shahzad, G. Medhi, R. E. Peale, W. R. Buchwald, J. W. Cleary, R. Soref, G. D. Boreman, and O. Edwards, J. Appl. Phys. **110**, 123105 (2011).
[16] S. Law, L. Yu, and D. Wasserman, J. Vac. Sci. Technol. B **31**, 03C121 (2013).
[17] S. Law, D. C. Adams, A. M. Taylor, and D. Wasserman, Opt. Express **20**, 12155 (2012).
[18] S. Law, L. Yu, A. Rosenberg, and D. Wasserman, Nano Lett. **13**, 4569 (2013).
[19] D. Li and C. Z. Ning, Opt. Express **19**, 14594 (2011).
[20] A. F. Oskooi, D. Roundy, M. Ibanescu, P. Bermel, J. D. Joannopoulos, and S. G. Johnson, Comput. Phys. Commun. **181**, 687 (2010).
[21] Lumerical Solutions Inc., http://www.lumerical.com/tcad-products/fdtd/.
[22] D. C. Adams, S. Inampudi, T. Ribaudo, D. Slocum, S. Vangala, N. A. Kuhta, W. D. Goodhue, V. A. Podolskiy, and D. Wasserman, Phys. Rev. Lett. **107**, 133901 (2011).
[23] See Supplemental Material at http://link.aps.org/supplemental/10.1103/PhysRevLett.112.017401 for details.
[24] M. Moharam, E. Grann, D. Pommet, and T. Gaylord, J. Opt. Soc. Am. A **12**, 1068 (1995).
[25] P. Yeh, A. Yariv, and C. Hong, J. Opt. Soc. Am. **67**, 423 (1977).
[26] S. Inampudi, I. Smolyaninov, and V. Podolskiy, Opt. Lett. **37**, 2976 (2012).